Metalicities of NGC 3256 using MIRI-MRS emission spectra

Yue Dong lady7214

April 7, 2024

Abstract

This study examines metallicity within NGC 3256, an ultra-luminous infrared galaxy, through the James Webb Space Telescope's Medium Resolution Spectroscopy. Focusing on neon, argon, sulfur, and iron emissions, we map elemental distributions with high precision, leveraging mid-infrared lines that are less affected by dust and temperature fluctuations. Our analysis offers a granular view of metallicity variations, contributing to our understanding of galaxy evolution, star formation histories, and interstellar metal transport. The findings emphasize JWST's impact in advancing galactic studies with its high-resolution infrared capabilities.

1 Introduction

The presence of heavier elements comes from stellar nucleosynthesis, where they are synthesized in the cores of stars and are spread through star wind and supernovae(SNe) into the interstellar medium(ISM). The ubiquitous metals in galaxies are studied to trace back the stars forming history and to understand their properties, i.e. luminosities, masses, and the exchange of metals between stars. The mass-metallicity relation, a key indicator of galaxy evolution (Tremonti et al, 2004), and metallicity gradients, crucial for understanding cosmological disk growth (Pilkington et al, 2012; Fu et al, 2009), underscore the importance of accurately determining spatial metallicity distributions in galaxies.

In this work, MIRI-MRS emission spectrums of a representative sample of local ultraluminous infrared galaxies(ULIRGs), i.e. NGC 3256(Figure 1), are observed. Previous Studies have already presented ISO SWS spectra of the starburst galaxy NGC 3256(*Rigopoulou et al, 1996*). With observation data presented by JWST over the full spectral range from 4.9 to 28.3 um at Medium Resolution Spectroscopy(MRS) mode, we captured emission spectrums at different star-forming areas in NGC 3256. The measurement investigates a finer internal structure of metallicity distribution within NGC 3256, linking spatial position to metallicity gradients. Appropriate corrections are applied where necessary.

Spatial distribution of neon, argon, sulfur and iron abundances is obtained using emission lines such as [MgV], and [NeII] with hydrogen recombination lines. The low extinction of MIR lines through galactic dust and independence on changes in electron temperature and density further justified the method.

2 Target and observation

MIRI/MRS data from the JWST archive is retrieved, and processed using the JWST calibration pipeline to produce the 12 sub-channel cubes with default spatial and spectral sampling. NGC 3256 is formed from a collision of two gas-rich progenitors, located about 100 million light years away. It is one of the brightest nearby galaxies ($\sim$40 Mpc) and the most luminous galaxy in the MIR region within redshift 0.01 from Earth. These features

Figure 1: NGC3256, NASA, ESA, Aaron S. Evans

Table 1: Fluxes of [SIII] emission lines

Identification	Wavelength λ (μm)	Dereddened Flux $\times 10^{-20} W cm^{-2}$
S II	18.89	112.2
S III	33.79	145.0

demonstrate that NGC 3256 is an excellent example to examine as a resolved galaxy observed by JWST.

3 Galaxy temperature and electron density

The electron density can be calculated from the ratio of two metal's emission flux. Here we choose the observed ratio of [SIII] at 18.71um and 33.47um, with z = 0.00935. The second emission line does not lie in the wavelength coverage of JWST (0.6 um to 28.5 um). Hence, to determine the electron density and temperature, we use the redden corrected fluxes of emission lines of [SIII] from 2.5-40 m ISO SWS spectra of the starburst galaxy NGC 3256(Table 1).

The best-fitting effective temperature T_{eff} 41000K ± 3000K (*Rigopoulou et al, 1996*) yields the electron density at 209.0 cm^{-3}. Varying the effective temperature from 38000K to 44000K, the electron density varies from 230.51 cm^{-3} to 190.85 cm^{-3}, computed with PyNeb.

Infrared lines offer many advantages over optical or ultraviolet (UV) lines for measuring elemental abundances, the most important of which is their small dependence on the electron temperature (*Bernard-Salas et al, 2001; Wu et al, 2008*).

4 Emission spectra

In this project, data are provided by JWST measurements. Thanks to the JWST's high resolution and its capability to detect in the mid-infrared range, we can capture detailed emission spectra of the galaxy. Here, we focus on three regions in NGC3256, demonstrated in Figure(2).

The intensities were estimated by fitting Gaussian profiles. I presented two fitting methods here: python fit and direct fit using Qfitsview. Additional PAH bands are also fitted using Lorenz curves. An Example of a Gaussian fit at 7.05 μm is presented in Figure(3). The parameters fitted through the two methods are with a percentage error at 8.7 % , hence are consistent with each other.

I carried out observations at the wavelengths of [Ar], [S], [Ne], and [Fe], helium and hydrogen spectral lines between 5.39 and 26.3 microns. A total of 14 lines were detected. The traditional equation to compute the Hbeta fluxes is given by Pottasch(1984) ,

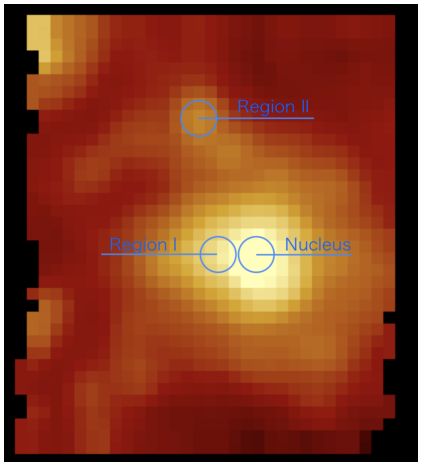

Figure 2: The regions in NGC3256: The nucleus, Region I and Region II

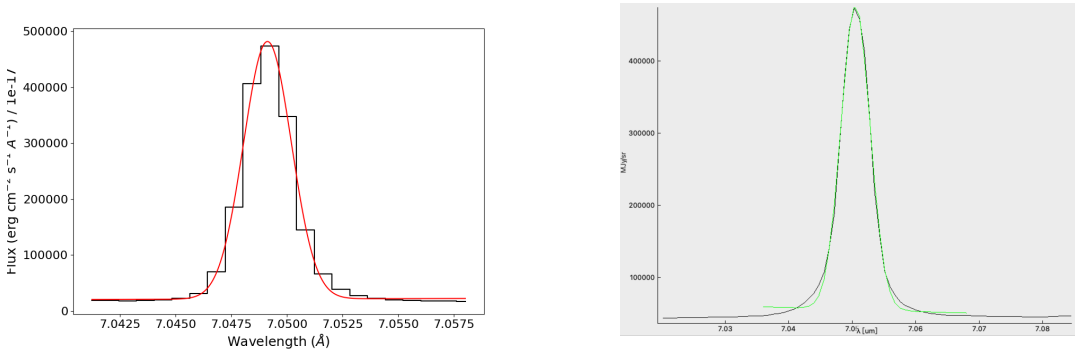

Figure 3: Gaussian fit at $7.05\mu m$ though python(left) and Qfitsview(right). The fitted results are consistent.

$$F(H_\beta) = \frac{S_\nu}{2.82 \cdot 10^9 \cdot t^{0.53} \left(1 + \frac{He^+}{H^+} + 3.7 \cdot \frac{He^{++}}{H^+}\right)} \tag{1}$$

but with observation directly through JWST, we can calculate the flux from the emission spectrum directly.

4.1 Emission spectrum at the nucleus

Figure(4) shows selected ionic, atomic and molecular lines observed in NGC 3256. Integrated line fluxes and their corresponding wavelengths as measured from the spectra are listed in Table(2).

From the emission line fluxes, we are able to compute the ionic metalicities of the galaxy.

5 Derivation of the metallicity abundances from PyNeb

The Pyneb module is developed to calculate the conditions of nebular plasma and the comparative abundance of elements by analyzing observed intensities of emission lines with an array of embedded extinction laws and corrections for ionization, assuming that the system is in equilibrium.

The Ionic abundance for an ion X^a is given by the following expression:

Table 2: The fluxes of emission lines

Line	wavelength λ (μm)	Flux(Nucleus) $\times 10^{-20} W cm^{-2}$	Flux(Region I) $\times 10^{-20} W cm^{-2}$	Flux(Region II) $\times 10^{-20} W cm^{-2}$
Fe II	5.391	0.890	0.746	0.418
Mg V	5.564	0.399	0.269	0.069
H2 S(5)	6.974	0.766	0.793	0.237
Ar II	7.051	24.790	19.012	2.184
HI(Pfa)	7.53	1.344	1.102	0.356
Ar III	9.075	2.222	1.681	1.013
H2 S(2)	12.394	1.429	1.333	1.550
Ne II	12.936	175.152	172.172	33.986
clorine	14.502	1.686	1.807	0.369
Ne III	15.700	16.961	14.323	5.622
H2 S(1)	17.196	2.288	3.435	4.336
Fe II	18.052	4.201	3.529	0.768
S III	18.888	65.972	95.106	22.284
Fe III	23.144	6.575	7.492	2.455
Fe II	26.232			2.807

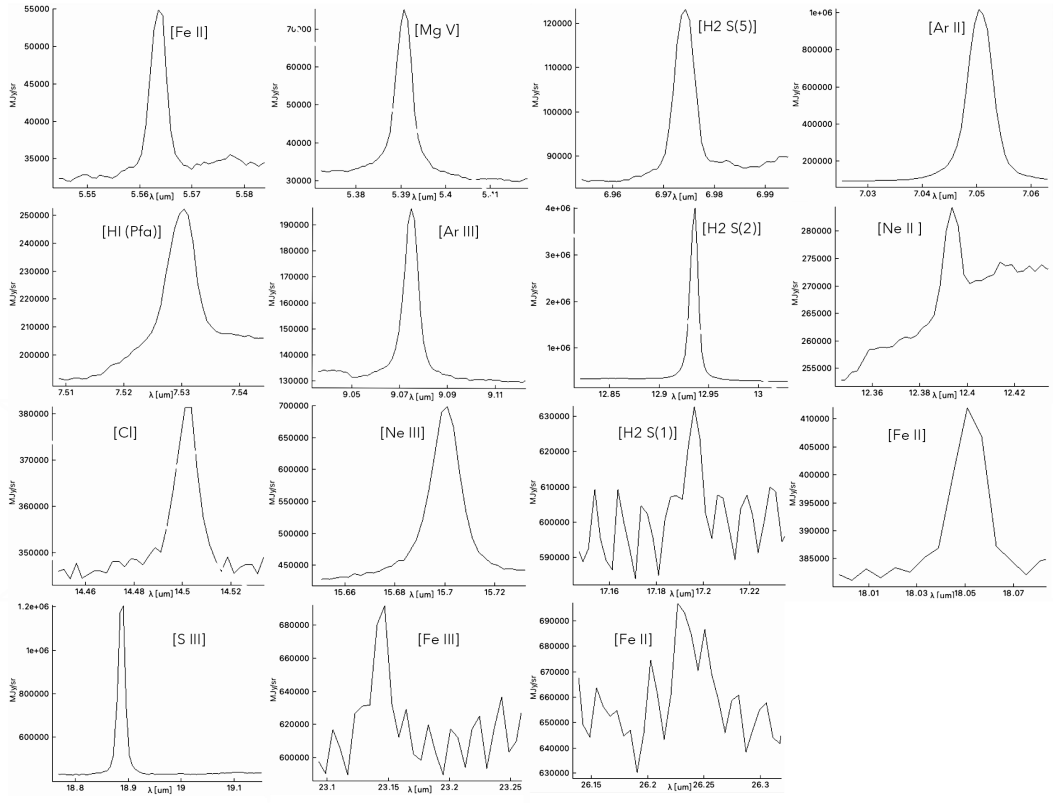

Figure 4: The line spectra for NGC 3256 at the nucleus, corresponding to Table 2

$$\frac{n\left(X^{a}\right)}{n\left(H^{+}\right)}=\frac{I\left(\lambda\right)}{I\left(H\beta\right)}\frac{\epsilon\left(H\beta\right)}{\epsilon\left(\lambda\right)} \tag{2}$$

where the I is the emission line intensity at a given wavelength and ϵ is the line emissivity, defined as

$$\epsilon_{ki}=n_{k}A_{ki}hc/\lambda \tag{3}$$

The emissivity is a function of n_k, the element density, A_{ki}, the radiative transition rate for levels $k \rightarrow i$ and the corresponding wavelength. Hence, the total element abundance X is simply the summation of each ionic abundance, which assumes an ionization correction factor(ICF) for the unseen ionic species.

Figure(5) demonstrates the different extinction correlations in PyNeb.

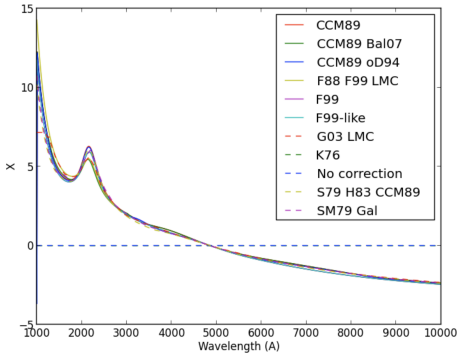

Figure 5: The extinction correlations

The emission spectrum in MIR range is insensitive to our choice of the extinction corrlation, as IR lights are less affected by extinction and less likely to be absorbed by dusts. Here, we choose the extinction correlation 'CCM89' from *Cardelli et al.*

The derived ionic abundances are reported in Table(3).

Table 3: Ionic abundances at different regions of NGC3256

Line	Region: Nucleus	Region: Region I	Region II	*Bernard-Salas et al*
Ar^{+}/H (10^{-6})	1.04	0.80	0.092	/
Ar^{++}/H (10^{-8})	8.23	6.22	3.75	/
Cl/H (10^{-8})	9.46	10.14	2.07	/
Mg/H (10^{-8})	4.46	3.01	0.78	/
Ne^{+}/H (10^{-4})	1.22	1.20	0.24	1.07
Ne^{++}/H (10^{-6})	5.516	4.66	1.83	6.40
S^{2+}/H (10^{-6})	3.34	4.81	1.13	3.21

Comparing the element abundance computed at the nucleus with others work, e.g. *Bernard-Salas et al, 2009*, we can show that the metalicity in Table3 is indeed accurate. Bernard-Salas'

study examines the element abundances over the entire NGC3256 using *Spitzer*/ IRS high-resolution 10 - 37 μm spectra. The study scans through the entire galaxy, instead of computing the metalicity of a small region within the galaxy. Hence, small deviation from the result of the study is reasonable.

5.1 Ionization correction function

In starburst galaxies, the most important stages of ionization of neon to determine the element abundances are Ne^{+} and Ne^{++}, which can be inferred from emission lines [NeII] and [NeIII]. Hence, no ICF function for Ne is needed(*Oli L et al, 2013*).

For sulfur, the its total abundance is derived adding the contribution from S^{2+} and S^{3+}. Notice that S^{2+} is measured here, but it's contribution is relatively small(*Martín-Hernández et al 2002, Vermeil and Van er Hulse 2002*).

The Fe abundance is hard to compute here, as the [FeIV] emission line wavelength doesn't lie in the range of JWST's observation scope, and the spectrum at the wavelength of [FeIII] is noisy to distinguish noise from ion emission fluxes.

5.2 Correlation between the ionic abundance and the distance from the nucleus

At the nucleus itself, indicated in Figure(6), metallicity is notably higher, indicating a rich concentration of elements heavier than hydrogen. Progressing to Region I and further into Region II, a decrease in the ionic abundance of these heavier elements relative to hydrogen is observed, evidenced by the lower heights of the bars in these regions. This trend suggests that the metallicity diminishes with increasing distance from the nucleus. The comparative decline in elements supports the notion that the nucleus region is more metal-rich, whereas the outer regions exhibit a more pronounced hydrogen presence.

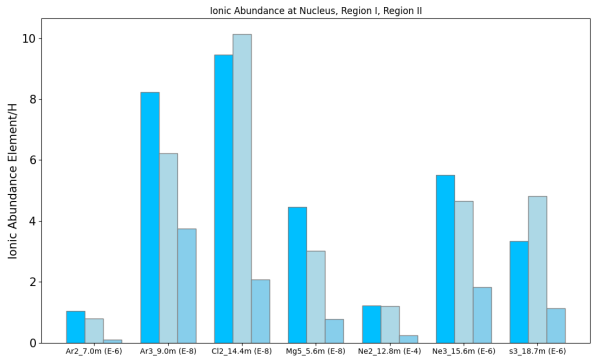

Figure 6: Ionic abundance at different regions

This gradient of metallicity is essential for understanding the compositional structure of the galaxies. To generalize these findings, further analysis across a broader range of regions and additional galaxies is essential. The JWST high-resolution spectroscopy will be pivotal in this expanded study, offering the precision needed to deepen our cosmic insights.

6 Conclusion

In conclusion, our study on NGC 3256's metallicities using the JWST's MIRI-MRS has provided valuable insights into metal distribution within ultra-luminous infrared galaxies. By analyzing emissions from neon, argon, sulfur, and iron, we have mapped elemental distributions with high precision, shedding light on the galaxy evolution. Our findings highlight the effectiveness of using mid-infrared lines for such analyses, thanks to their minimal dust extinction and temperature fluctuation effects, showcasing the JWST's capabilities in advancing galactic studies. This work paves the way for future research into metallicity gradients across various galaxies, promising to deepen our understanding of the universe's underlying processes.

7 Appendix

7.1 Codes

Code and related data sources are on https://github.com/Florencia12345/Y2-Extra-Project.git.

References

[1] Tremonti, C. A., Heckman, T. M., Kauffmann, G., Brinchmann, J., Charlot, S., White, S. D., Seibert, M., Peng, E. W., Schlegel, D. J., Uomoto, A., Fukugita, M., Brinkmann, J. (2004). The Origin of the Mass–Metallicity Relation: Insights from 53,000 Star-Forming Galaxies in the SDSS. ArXiv. https://doi.org/10.1086/423264

[2] Pilkington, K., Few, C. G., Gibson, B. K., Calura, F., Thacker, R. J., Molla, M., Matteucci, F., Rahimi, A., Kawata, D., Kobayashi, C., Brook, C. B., Stinson, G. S., Couchman, H. M., Bailin, J., Wadsley, J. (2012). Metallicity Gradients in Disks: Do Galaxies Form Inside-Out? ArXiv. https://doi.org/10.1051/0004-6361/201117466

[3] Rigopoulou, D., "SWS spectroscopy of the starburst galaxy NGC 3256.", ¡i¿Astronomy and Astrophysics¡/i¿, vol. 315, pp. L125–L128, 1996.

[4] The ISO–SWS spectrum of planetary nebula NGC 7027, J. Bernard-Salas, S. R. Pottasch, D. A. Beintema and P. R. Wesselius, AA, 406 1 (2003) 175, DOI: https://doi.org/10.1051/0004-6361:20030797

[5] Cardelli, J. A., Clayton, G. C., and Mathis, J. S., "The Relationship between Infrared, Optical, and Ultraviolet Extinction", ¡i¿The Astrophysical Journal¡/i¿, vol. 345, IOP, p. 245, 1989. doi:10.1086/167900.

[6] Oli L. Dors, Guillermo F. Hägele, Mónica V. Cardaci, Enrique Pérez-Montero, Ângela C. Krabbe, José M. Vílchez, Dinalva A. Sales, Rogério Riffel, Rogemar A. Riffel, Optical and mid-infrared neon abundance determinations in star-forming regions, Monthly Notices of the Royal Astronomical Society, Volume 432, Issue 3, 01 July 2013, Pages 2512–2528, https://doi.org/10.1093/mnras/stt610

[7] Probing AGB nucleosynthesis via accurate Planetary Nebula abundances, P. Marigo, J. Bernard-Salas, S. R. Pottasch, A. G. G. M. Tielens and P. R. Wesselius, AA, 409 2 (2003) 619-640, DOI: https://doi.org/10.1051/0004-6361:20030953